

PHASE NOISE AMPLITUDE DEPENDENCE IN SELF-LIMITING WINE-GLASS DISK OSCILLATORS

Seungbae Lee and Clark T.-C. Nguyen

Center for Wireless Integrated Microsystems(WIMS)
 Department of Electrical Engineering and Computer Science
 University Of Michigan Ann Arbor, Michigan 48109-2122, U.S.A.
 Tel.:(734)764-3352, Fax:(734)647-1781, email:seungbae@umich.edu

ABSTRACT

Self-limiting 46.4-MHz series resonant reference oscillators employing a wine-glass mode disk micromechanical resonator to avoid hard limiting without the need for ALC have achieved measured phase noises of -113 and -134 dBc/Hz at 1kHz and far-from-carrier offsets, respectively. When divided down to 10MHz frequency for fair comparison with other oscillators, these values correspond to -126 dBc/Hz and -147 dBc/Hz, which now satisfy specifications for low-end cellular handsets. For these oscillators, $1/f^3$ phase noise is found to be independent of vibration amplitude for amplitudes below critical Duffing, which pares down the list of possible mechanisms to those that are amplitude independent.

I. INTRODUCTION

Although their exceptional Q ($>10,000$) and superb thermal and aging stability make quartz crystals the resonators of choice for precision reference oscillators in portable applications [1], their size and incompatibility with integrated circuits preclude true system-on-a-chip wireless solutions. On the other hand, electrostatically transduced vibrating micromechanical (“ μ mechanical”) resonators have become increasingly attractive as frequency-setting elements in reference oscillators for communication applications due to their potential for direct integration or bonded merging with transistors onto single chips [2]-[5]. In particular, phase noise performance nearing the requirements of the GSM cellular telephone standard have recently been demonstrated via an oscillator referenced to an extensional-mode single-crystal silicon vibrating bar with a Q of 200,000, constructed using a thick-device-layer SOI process [6]. Although the resonator used in [6] lacked adequate temperature stability, another resonator based on surface micromachined polysilicon structural material was recently demonstrated with a temperature coefficient as low as -0.24 ppm/ $^{\circ}$ C [7], a Q of 4,000 at 10 MHz, and a proven integrability with transistor electronics [2][5]. However, an oscillator based on this polysilicon resonator exhibited a $1/f^3$ phase noise component farther from the carrier than expected that prevented the oscillator from achieving GSM-like phase noise specifications (e.g., for 10 MHz reference oscillator, better than -120 dBc/Hz at 1kHz offset frequency, -130 dBc/Hz preferred) [8].

Recently, automatic level control (ALC) circuitry designed to limit the vibration amplitude of a micromechanical resonator in an oscillator has been found to successfully remove this $1/f^3$ phase noise [9], suggesting resonator transducer or mechanical nonlinearity as the source of this noise. Unfortunately, ALC removes $1/f^3$ noise at the price of carrier power, so the phase noise performance of ALC’ed oscillators still falls well below the needs of today’s cellular wireless standards [9]. In addition, although a mechanism

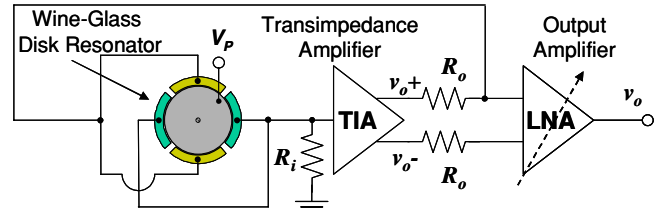


Fig. 1: Schematic of the series oscillator with transimpedance sustaining amplifier utilizing a wine-glass mode disk resonator tank.

linked to resonator amplitude has been identified, an analytical model that accurately predicts the measured $1/f^3$ component has so far been elusive.

Pursuant to both better understanding the source of $1/f^3$ noise and achieving better overall phase noise performance, this work harnesses a recently demonstrated polysilicon wine-glass mode vibrating disk resonator with high- Q even in air [10], and with higher power handling ability (i.e., linearity) than previous surface-micromachined resonators, to attain oscillators that self-limit before critical point Duffing nonlinearity without the need for ALC. By avoiding hard nonlinearity, these oscillators achieve 10-MHz-effective phase noises of -123 dBc/Hz at 1kHz offset and -147 dBc/Hz far-from-carrier under atmospheric pressure, which now satisfy specifications for some cellular handsets. Equally importantly, these oscillators also provide better insight into the amplitude dependence (or independence) of $1/f^3$ phase noise.

II. OSCILLATOR TOPOLOGY AND OPERATION

Like a previous oscillator design [9], the oscillator of this work uses a series resonant topology, shown in Fig. 1, in which the wine-glass disk is embedded in a positive feedback loop together with an off-chip NE5211 transresistance sustaining amplifier possessing sufficient gain to initiate and sustain oscillation. As shown, since the micromechanical resonator used for this work is a multi-port device (as opposed to the one port devices used in previous work [8][9]), the dc-bias voltage V_p is directly connected to the resonator structure without the need for the bias tee used in [8][9]. Other than this and the use of a more advanced micromechanical resonator, the criteria governing start-up and sustenance of oscillation are identical to those described in [9]:

1. For Start-Up: $R_{amp} > R_x + R_i + R_o$
2. In Steady-State: $R_{amp} = R_x + R_i + R_o$
3. Loop Phase Condition: 0° around the positive feedback loop

where R_{amp} , R_i , and R_o are the gain, input resistance, and output resistance, of the transresistance sustaining amplifier, respectively; and R_x is the series motional resistance of the wine-glass disk. As

Travel Support has been generously provided by the Transducers Research Foundation and by the DARPA MEMS and DARPA BioFlips programs.

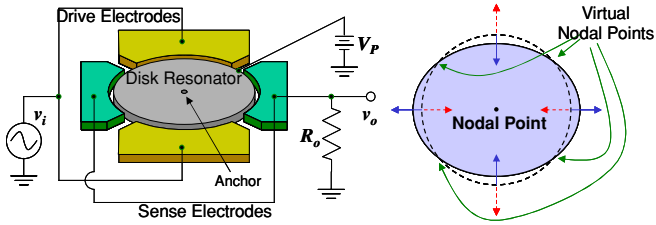


Fig. 2: (a) Perspective-view of a wine-glass disk resonator illustrating a typical two-port bias and excitation scheme, and (b) its mode shape.

will be described, this oscillator limits when its resonator R_x increases with amplitude to the point of satisfying criterion 2 above.

III. RESONATOR AMPLITUDE LIMITATIONS

Fig. 2(a) presents a more detailed schematic of the disk resonator with electrodes configured to excite the fundamental wine-glass mode shape shown in Fig. 2(b). The dc-bias voltage V_p applied to the disk effectively amplifies the force and motional output current induced when a resonance ac excitation voltage v_i forces the disk into resonance vibration. The motion is constrained entirely to the plane of the disk, with its perimeter expanding along one axis and contracting in the orthogonal axis about the center point, which remains stationary, acting as a node. Although four additional quasi-nodal points exist on the disk perimeter and thereby allow greater flexibility in the choice of support structure [10], this work simply anchors the disk at its center in order to maximize the available electrode area. The wine-glass resonance frequency f_o , goes as the inverse of its radius R , and can be obtained by solving the mode frequency equation given in [10]

At the amplitudes experienced during oscillator vibration, the force F needed to achieve a given vibration amplitude x for this electrostatically driven resonator becomes of a function of third-order Duffing nonlinearity [11] and is governed by the expression

$$\frac{F}{m_r} = \ddot{x} + \frac{\omega_o}{Q} \dot{x} + \frac{k_1}{m_r} x - \frac{k_3}{m_r} x^3 = \ddot{x} + \frac{\omega_o}{Q} \dot{x} + \omega_o^2 (x - \mu x^3) \quad (1)$$

$$\text{where, } k_1 = k_{m1} - k_{e1}, \quad k_3 = k_{e3} - k_{m3}, \quad \omega_o = \sqrt{\frac{k_1}{m_r}}, \quad \mu = \frac{k_3}{k_1} \quad (2)$$

and where m_r is effective mass of resonator; k_{m1} and k_{e1} are the linear mechanical and electrical spring constants, respectively; and k_{m3} and k_{e3} model their third-order spring nonlinearities. For the resonators of this work, the electrode-to-resonator gaps d_o are quite small, so $k_{e3} > k_{m3}$ (i.e., the third-order coefficient in (1) is negative), so *spring softening* occurs as the vibration amplitude increases. The resonance frequency then decreases as the resonator amplitude increases, resulting in a frequency response curve that bends leftward as amplitudes increase, as illustrated in Fig. 3, where the amplitude dependence of the peak (radian) frequency ω is governed by the expression [11]

$$\omega^2 = \omega_o^2 - \frac{3}{4} \frac{k_3}{m_r} x^2 \quad (3)$$

where ω_o is the radian resonance frequency at small amplitudes.

When the peak vibration amplitude exceeds the critical point:

$$X_{crit} \approx \frac{1.52}{\sqrt{\mu Q}} \quad (4)$$

the amplitude versus frequency curve bends to a point where there

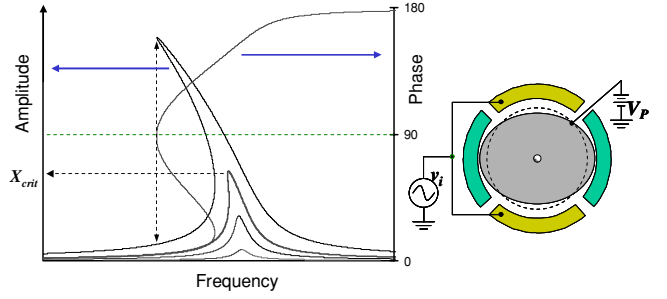


Fig. 3: Schematic depiction of the theoretical Duffing curve expected for large amplitudes.

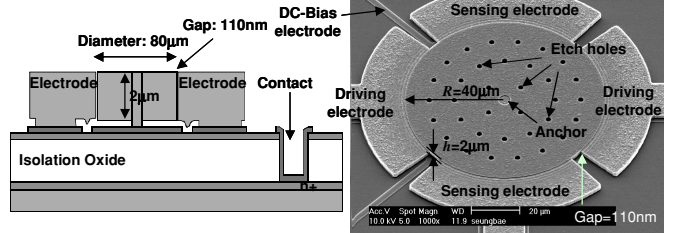


Fig. 4: Cross section and SEM of a 46.4-MHz wine-glass mode disk polysilicon resonator, with dimensions indicated.

are three theoretically valid amplitudes for each frequency in the bent portion of the curve. This amplitude ambiguity leads to unstable steady-state operation [2], which then results in excessive phase noise. Needless to say, operation at amplitudes past the critical point are not recommended, so X_{crit} effectively defines an amplitude threshold that then sets the maximum rms power handling ability of the resonator to

$$P_o = \frac{1}{2} \frac{\omega_o k_1}{Q} x^2 \leq \frac{1}{2} \frac{\omega_o k_1}{Q} X_{crit}^2 = 1.16 \frac{\omega_o k_1}{\mu Q^2} \quad (5)$$

IV. EXPERIMENTAL RESULTS

46.4-MHz polysilicon wine-glass mode disk resonators were designed and fabricated using a process similar to a previously reported self-aligned stem process [12], except for the use of a chemical mechanical polishing (CMP) step to reduce topography at the end of the process. Fig. 4 presents the final cross section and scanning electron micrograph (SEM) of one such resonator, identifying key features and dimensions. With 80- μm diameters, the disks of this work are larger than previous ones, so etch holes are now used to keep release etch times under 15 minutes. This is needed to prevent HF attack of the nitride isolation layer underneath the devices, which occurs when the nitride is exposed to 49 wt.% HF for longer than 35 minutes. Structurally, the etch holes reduce the resonator stiffness, resulting in a slight reduction of its resonance frequency. Finite element simulation using ANSYS predicts frequencies of 46.7-MHz and 48.1-MHz for wine-glass mode disk resonators with and without etch holes, respectively.

Fig. 5 presents frequency spectra measured for the device of Fig. 4 under 50 mTorr pressure in a custom-built vacuum chamber, and in air as well, where the dependence of frequency on dc-bias-derived electrical stiffness [13] and on increased gas damping in air can be clearly seen. In vacuum, the Q is 30,267. In air, although a larger dc-bias V_p is needed to achieve the same motional resistance, the Q is still a respectable 5,091. The oscillator circuit of Fig. 1 was implemented on a printed circuit (pc) board shaped to allow placement within the custom-built vacuum chamber. Dies containing fabricated wine-glass mode disk resonators were glued to this

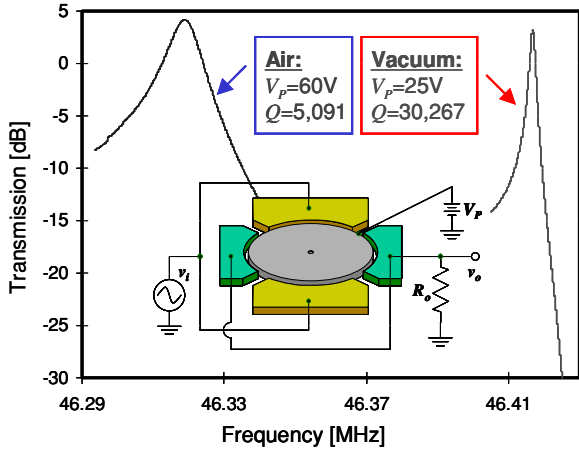


Fig. 5: Measured frequency characteristics for the wine-glass mode disk resonator in air as well as in vacuum, with an inset specifying the measurement setup.

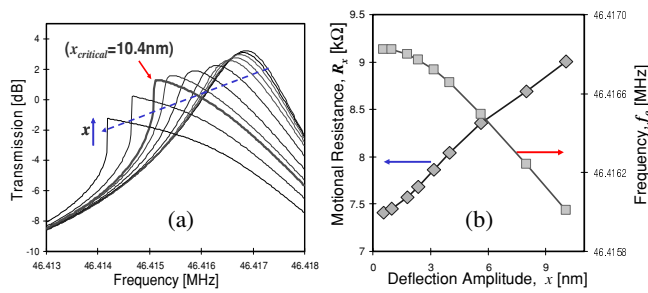


Fig. 6: Measured plots summarizing the displacement amplitude dependence of the wine-glass disk resonator: (a) frequency responses, showing Duffing nonlinearity; and (b) motional resistance R_x and resonance frequency; all measured under 50 mTorr vacuum.

board over specially grounded regions and bonded to board-mounted electronics.

Fig. 6(a) presents measured plots of transmission versus frequency for a 46.4-MHz wine-glass mode disk under increasing drive force amplitudes, where spring softening Duffing behavior is clearly seen. In particular, the peak frequency clearly decreases with increasing displacement amplitude. In addition, a decrease in peak transmission is also seen, consistent with [2], where either Q or transducer electromechanical coupling, or both, may be decreasing with displacement amplitude. This reduction in transmission corresponds to an increase in series motional resistance R_x with displacement amplitude, plotted in Fig. 6(b) (along with frequency), which then provides a convenient mechanism for self-limiting of an oscillator referenced to a wine-glass mode micro-disk. In particular, at oscillator start-up, when the R_x of the resonator is smaller than the transresistance gain of the sustaining amplifier R_{amp} , the overall loop gain is greater than unity, so oscillations build up. As the amplitude of the resonator grows, however, R_x grows until it equals R_{amp} minus other series loop resistances (e.g., amplifier input and output resistance), at which point, the oscillation amplitude stops growing, and steady-state operation is achieved. In this mode of operation, the steady-state oscillation amplitude can be set by setting the initial difference between R_x and R_{amp} , which can in turn be set by choice of dc-bias voltage V_p [9]. The wine-glass disk of this work has an advantage over other resonators in that its power handling and R_x versus amplitude characteristic are such that oscillation with sufficient output power can be achieved at vibration amplitudes well below critical Duffing, which is one of

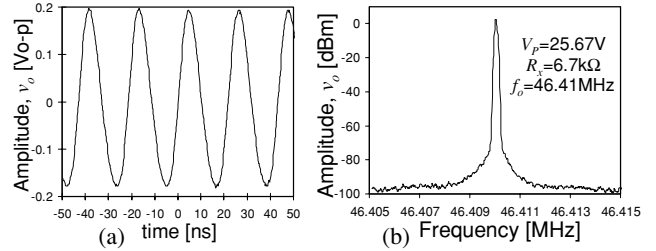


Fig. 7: Measured output (a) waveform and (b) Fourier spectrum for the self-limiting wine-glass disk micromechanical oscillator.

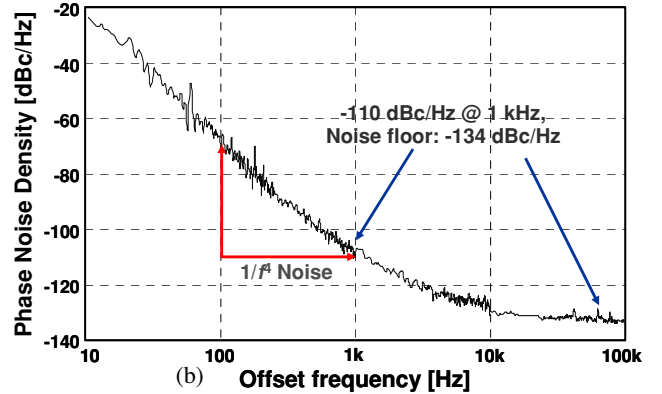
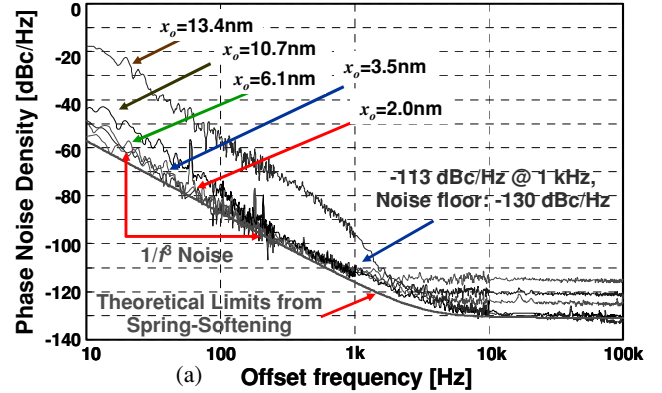


Fig. 8: Measured phase noise density-to-carrier power ratio versus carrier offset frequency for the μ mechanical resonator oscillator in (a) vacuum and (b) in atmosphere.

the criteria for good oscillator stability in Section III.

Fig. 7 presents the measured output waveform and Fourier spectrum for a self-limiting wine-glass disk oscillator hooked up as in Fig. 1 and operated under conditions summarized in the inset. Fig. 8 presents plots of phase noise density versus frequency offset for the 46.4-MHz wine-glass disk oscillator, with displacement amplitude as a third variable, measured (a) under 50 mTorr vacuum and (b) in air, using an HP E5500 Phase Noise Measurement System. Operational specifics for each curve are summarized in Table I. In vacuum, a $1/f^3$ component is seen close to the carrier, and this noise clearly depends upon the oscillation amplitude, becoming considerably worse when the amplitude of oscillation becomes larger than the critical Duffing amplitude (10.4 nm), where multiple operating amplitudes are possible in the curves of Fig. 6(a), verifying that operation past the critical point should be avoided.

In vacuum, the phase noise at 1kHz offset from the carrier is of the $1/f^3$ variety, as expected, but curiously it remains fairly constant at -113 dBc/Hz for amplitudes below the critical amplitude. On the other hand, the far-from-carrier phase noise has a rather strong

Table I. Operational Data for Various Oscillation Amplitudes

Amplitude, x [nm]	2.0	3.5	6.1	10.7	13.4
V_p [V]	24.54	24.67	24.93	25.67	26.96
R_x [k Ω]	7.323	7.245	7.095	6.691	6.066
f_o [MHz]	46.4131	46.4124	46.4116	46.4093	46.3990
v_i [mV]	34.6	61.5	109.4	194.5	259.4
$L[f_m=1\text{kHz}]$	-111	-111	-112	-113	-97
Noise Floor	-115.2	-121.4	-125.3	-130.5	-132.3

dependence on amplitude, getting smaller with larger displacement amplitude, and attaining its lowest value of -130 dBc/Hz at an amplitude of 10.7 nm, right at the edge of critical Duffing. When divided down to 10MHz for fair comparison with other standard oscillators, the phase noise for the 10.7 nm displacement case at 1kHz and far-from-carrier offsets are -126 and -143 dBc/Hz, respectively, which are now in the range of acceptable values for cellular handsets, although some sticklers might still demand -130 and -150 dBc/Hz. If needed, these values should be attainable via a redesign to provide a more favorable Duffing response curve (e.g., by optimizing the electrode-to-resonator gap spacing).

In air (Fig. 8(b)), although a mysterious $1/f^4$ phase noise component introduces itself at carrier offset frequencies below 1kHz, the overall performance of the oscillator matches that of the vacuum-operated version past 1kHz, despite its lower Q . The performance even exceeds that in vacuum at far-from-carrier offsets, achieving 4dB better in this region. The reason: In air the amplitude required to make $R_x=R_{amp}$ is smaller than that needed in vacuum, and the dc-bias voltage V_p needed is larger—a combined condition that allows both small displacement amplitude for good close-to-carrier phase noise, but large current output amplitude (provided by the larger V_p) for good far-from-carrier noise.

V. INSIGHTS INTO $1/f^3$ PHASE NOISE

The observation that $1/f^3$ phase noise is independent of vibration amplitude for amplitudes below critical Duffing pares down the list of possible mechanisms to those that are amplitude independent. Among these mechanisms is the previously proposed [8] shaping of aliased $1/f$ noise by the resonator passband, leading to a $1/f^3$ phase noise component governed by

$$L[f_m] = \left[\frac{1}{4Q_i^2 V_p^2} + \frac{1}{4k_1^2} \frac{(\epsilon_o A_o)^2}{d_o^6} V_p^2 \right] \cdot 2qK_1 I_B R_{amp}^2 \frac{f_o^2}{f_m^3} \quad (6)$$

where d_o and A_o are the electrode-to-resonator gap and overlap area, respectively; and $K_1(50\text{kHz})$ and $I_B(50\mu\text{A})$ are the $1/f$ noise constant and base current, respectively, of the bipolar transistor at the input of the sustaining transimpedance amplifier with gain R_{amp} , 14 k Ω .

Another possible mechanism arises when $1/f$ noise on the dc-bias voltage V_p leads to electrical-stiffness-induced frequency instability, which then generates a $1/f^3$ phase noise component governed by

$$L[f_m] \approx \frac{1}{2} \left(\frac{\epsilon_o A_o V_p}{k_{m1} d_o^3} \right)^2 2qK_1 I_B R_{amp}^2 \frac{f_o^2}{f_m^3} \quad (7)$$

Unfortunately, neither of the above equations exactly matches the measured phase noise of Fig. 8. In particular, using the data in the 4th column of Table I, (6) predicts -124 dBc/Hz at 1 kHz offset, while (7) yields -120 dBc/Hz—each more than -7 dBc/Hz from the

measured value. A new formulation based on frequency shifts due to Duffing distortion (3) leads to the expression

$$L[f_m] \approx \frac{1}{(2\pi)^4 f_o^2} \cdot \left(\frac{3k_3}{4m_r} \right)^2 \frac{4Q^2 V_p^2}{k_1^2} \cdot \frac{(\epsilon_o A_o)^2}{d_o^6} \cdot 2qK_1 I_B R_s^2 \cdot \frac{x^4}{f_m^3} \quad (8)$$

This expression yields -115 dBc/Hz at 1kHz using the data in the 4th column of Table I, which is very close to the measured value. However, this expression also exhibits a dependence on amplitude not seen in measurement, so cannot be entirely correct.

Perhaps the previous observation that ALC or limiting via electronics rather than the resonator eliminates $1/f^3$ phase noise is more telling. In particular, the mechanism for $1/f^3$ phase noise is likely tied to the Duffing distortion-based limiting mechanism described in Section III. Efforts to properly model $1/f^3$ phase noise are ongoing.

VI. CONCLUSIONS

A 46.4-MHz μ mechanical resonator reference oscillator has been demonstrated using a series resonant oscillator topology in which a transimpedance amplifier with zero phase shift sustains the oscillation of a high stiffness wine-glass mode μ mechanical disk resonator. Due to the high- Q , high power handling, and large stiffness (relative to previous micromechanical devices), of the wine-glass disk resonator, this oscillator achieves a phase noise performance consistent with the needs of commercial wireless communications without the need for ALC. This performance is attained as long as the vibration amplitude of the resonator is kept below the critical Duffing amplitude; otherwise, excessive phase noise ensues. In addition, without ALC or some electronic means for limiting, this oscillator still exhibits the $1/f^3$ close-to-carrier phase noise seen in previous micromechanical oscillators, further verifying that limiting via resonator nonlinearity (e.g., Duffing-related nonlinearity) is likely responsible for this noise. The fact that $1/f^3$ noise is found to be independent of vibration amplitude for operation below critical Duffing sheds more light on the roots of this noise phenomenon.

Acknowledgment: This work was supported under DARPA Cooperative Agmt. No. F30602-01-1-0573.

References:

- [1] R. J. Matthys, *Crystal Oscillator Circuits*. New York: Wiley, 1983.
- [2] C. T.-C. Nguyen, *et al.*, *IEEE J. Solid-State Circuits*, vol. 34, no. 4, pp. 440-455, April 1999.
- [3] T. A. Core, *et al.*, *Solid State Technology*, pp. 39-47, Oct. 1993.
- [4] A. E. Franke, *et al.*, *Tech. Digest*, 12th Int. IEEE MEMS Conf., Orlando, Florida, Jan. 17-21, 1999, pp. 630-637.
- [5] A.-C. Wong, *et al.*, *Dig. of Tech. Papers*, Transducers'01, Munich, Germany, June 10-14, 2001, pp. 992-995.
- [6] T. Mattila, *et al.*, *Sensors and Actuators*, A 101, pp. 1-9, 2002.
- [7] W. -T. Hsu, *et al.*, *Tech. Digest*, 2002 IEEE Int. Micro Electro Mechanical Systems Conf., Jan. 20-24, 2002, pp. 731-734.
- [8] S. Lee, *et al.*, *Digest of Technical Papers*, Transducers'01, Munich, Germany, June 10-14, 2001, pp. 1094-1097.
- [9] S. Lee, *et al.*, *Proceedings of 2003 IEEE Frequency Control Symposium*, Tampa, Florida, May 5-8, 2003, pp.341-349.
- [10] M. A. Abdelmoneum, *et al.*, *Technical Digest*, 16th Int. IEEE Micro Electro Mechanical Systems Conf., 2003, pp. 698-701.
- [11] S. Timoshenko, D. H. Young, and W. Weaver Jr., *Vibration Problems in Engineering*. 5th ed. New York: Wiley, 1990.
- [12] J. Wang, *et al.*, *Dig. of Tech. Papers*, Transducers'03, 2003, pp. 947-950.
- [13] F. D. Bannon III, *et al.*, *IEEE J. Solid-State Circuits*, vol. 35, no. 4, pp. 512-526, April 2000.